THE JOURNAL OF PHYSICAL CHEMISTRY Letters

Letter

pubs.acs.org/JPCL

Stability of Porous Platinum Nanoparticles: Combined In Situ TEM and Theoretical Study

Shery L. Y. Chang,*[,†,⊥] Amanda S. Barnard,*[,‡] Christian Dwyer,[†,¶] Thomas W. Hansen,[§] Jakob B. Wagner,[§] Rafal E. Dunin-Borkowski,[§,#] Matthew Weyland,[†,¶] Hiromi Konishi,[∥] and Huifang Xu[∥]

[†]Monash Centre for Electron Microscopy, [⊥]School of Chemistry, and [¶]Department of Materials Engineering, Monash University, Clayton, Australia

[‡]Virtual Nanoscience Laboratory, CSIRO Materials Science and Engineering, Clayton, Australia

[§]Center for Electron Nanoscopy, Technical University of Denmark, Denmark

[∥]Department of Geoscience, and Materials Science Program, University of Wisconsin−Madison, Madison, Wisconsin, United States

[#]Ernst Ruska-Centre for Microscopy and Spectroscopy with Electrons, Peter Gruenberg Institute, Research Centre, Juelich, Germany

Supporting Information

ABSTRACT: Porous platinum nanoparticles provide a route for the development of catalysts that use less platinum without sacrificing catalytic performance. Here, we examine porous platinum nanoparticles using a combination of in situ transmission electron microscopy and calculations based on a first-principles-parametrized thermodynamic model. Our experimental observations show that the initially irregular morphologies of the as-sythesized porous nanoparticles undergo changes at high temperatures to morphologies having faceted external surfaces with voids present in the interior of the particles. The increasing size of stable voids with increasing temperature, as predicted by the theoretical calculations, shows excellent agreement with the experimental findings. The results indicate that hollow-structured nanoparticles with an appropriate void-to-total-volume ratio can be stable at high temperatures.

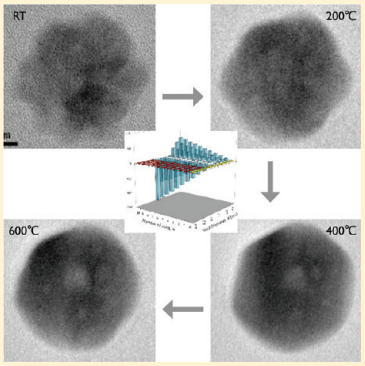

SECTION: Physical Processes in Nanomaterials and Nanostructures

Platinum and platinum-based bimetallic nanoparticles continue to find application in a plethora of industrial scenarios. For example, they are used as critical components in automobile catalytic converters,[1] in the petroleum industry for a number of catalytic re-forming processes,[2] and as electrocatalysts for PEM fuel cells.[3,4] The activity of such nanoparticle catalysts is largely dependent on the accessible surface area of the nanoparticles. In the case of platinum-based nanoparticles, particles smaller than 10 nm dispersed on support materials, such as carbon black, silicon oxide, titanium oxide, and aluminum oxide, are used to achieve high activity. However, while platinum-based catalysts achieve excellent performance, platinum is an extremely rare metal (<0.003 ppb in the earth's crust) with a correspondingly high price. Hence, reduction of the amount of platinum used in platinum-based catalysts, without sacrificing catalytic performance, is a major pursuit in the development of new catalysts.

Several current strategies exist for reducing the amount of platinum used. These include the synthesis of subnanometer platinum clusters,[5,6] engineering nanoparticles of specific shapes for increased activity,[7−9] and the addition of secondary metals to reduce both the platinum content and the degree of poisoning.[10−12] Another increasingly important strategy is to increase the surface-area-to-volume ratio by means of porous nanostructured particles. Porous nanostructures can be synthesized using a variety of approaches, including the use of templates to generate mesoporous[13] and dendritic structures,[14,15] colloidal methods to generate hollow structures,[16−18] and self-organization and other methods to generate dispersed porous nanoparticles.[19−21] Porous-structured platinum particles not only possess a greater surface area, but more importantly, they contain additional sites for the reactions.[21] These advantages have been evidenced through their higher catalytic activity over conventional platinum particles.[19−21]

On the other hand, platinum particles are known to sinter at high temperatures, which is unfortunate given that most of the chemical reactions happen at elevated temperatures (typically between 150 and 500 °C but up to 1000 °C in combustion conditions). Sintering causes both a reduction in the surface area and changes to the particle morphologies, and it is a major factor in the deactivation of nanoparticle catalysts. Hence, while porous nanostructured particles may provide economic advantages over solid particles of the same diameter, their usefulness is assured only if they are thermodynamically stable

Received: February 13, 2012
Accepted: March 27, 2012
Published: March 27, 2012

   dx.doi.org/10.1021/jz3001823 | J. Phys. Chem. Lett. 2012, 3, 1106−1110

under the temperatures relevant to catalysis. An important step toward resolving the dilemma is to establish an understanding of the stability of porous nanoparticles as a function of temperature.

Here, we present a study of the atomic-scale evolution of porous platinum nanoparticles at several temperatures up to 600 °C. The porous Pt nanoparticles were synthesized using a two-step process[22] (see the Supporting Information for details). To study the structural and morphological changes to the porous nanoparticles at elevated temperatures, we have used aberration-corrected in situ transmission electron microscopy (TEM), which allows us to image changes in nanoparticles in a controlled environment without the influence of ex situ factors. The use of an aberration-corrected TEM enables higher spatial resolution and increased accuracy in the interpretation of structural changes of the nanoparticles. To explain the experimental observations, we have carried out thermodynamic modeling based on first-principles calculations using parameters matching the experimental conditions.

Figure 1 shows representative high-resolution TEM (HRTEM) images of the as-synthesized porous Pt particles.

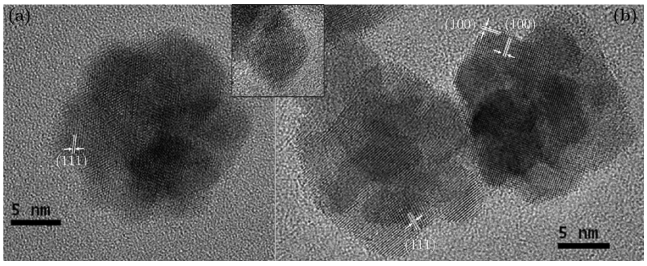

Figure 1. Aberration-corrected HRTEM images of as-synthesized porous platinum particles. A single-crystalline primary particle is shown in the inset.

The particles have sizes in the range of 18−19 nm, and are comprised of single-crystal primary particles 5.5 nm in size. Primary particles are octahedrally shaped, as shown in the inset in Figure 1. We have also found a small fraction of the primary particles that are truncated octahedron shaped. The shapes of these primary particles are in agreement with our previous experimental observations[23−26] as well as recent theoretical and experimental reports.[27−29]

To establish the thermal stability of the porous nanoparticles, that is, the effect of temperature on the porous nanostructures, the particles were heated in situ under vacuum in the aberration-corrected TEM. Figure 2 shows the morphological evolution of a single nanoparticle from room temperature up to 580 °C over a time frame of 4 h (the room-temperature image is shown in Figure 1a). At room temperature, the shape of the particle is quasi-spherical with an irregular external surface, as expected for a porous nanoparticle. With increasing temperature up to 300 °C, the external surfaces gradually became smoother, and the {111} and {100} facets begin to define the exterior shape (Figure 2a−c). At 400 °C, the particle becomes well-faceted, forming a shape close to a truncated octahedron with a very small fraction of {110} surfaces (surface planes were determined using Fourier transforms of the HRTEM images), as shown in Figure 2d. For temperatures between 400 and 580 °C, the morphology of the particle remains unchanged (Figure 2d−f).

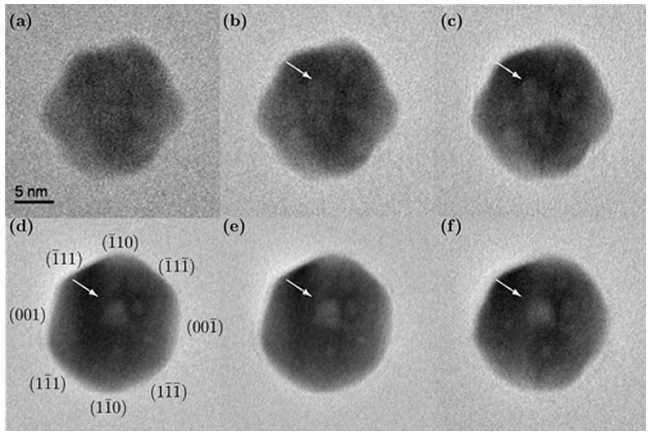

Figure 2. Selected temperature sequence of a single particle shown in Figure 1a, taken in situ in an aberration-corrected TEM at 300 kV: (a) 120, (b) 220, (c) 300, (d) 400, (e) 500, and (f) 580 °C. The surface facets seen edge-on are labeled in (d), and the voids are marked with white arrows.

While the external surfaces of the nanoparticles became well-faceted with increasing temperature, the porous nanoparticles, unexpectedly, do not sinter to form solid nanoparticles. Instead, we found that voids exist in the interior of the majority of nanoparticles at higher temperatures, and we observe changes in these voids with increasing temperature. For example, in the case of the nanoparticle considered above, at 300 °C, there are voids of approximately 1.5 nm in size within the particle (Figure 2c). Upon increasing the temperature to 400 °C, voids in close proximity coalesce to form larger voids (Figure 2d). For temperatures between 400 and 580 °C, these larger voids remain stable (Figure 2d−f).

Figure 3 provides another example of the temperature-dependent morphology of the porous Pt nanoparticles. Although in this case the nanoparticle is in contact with neighboring nanoparticles, we nonetheless observe trends similar to the previous example of an isolated nanoparticle.

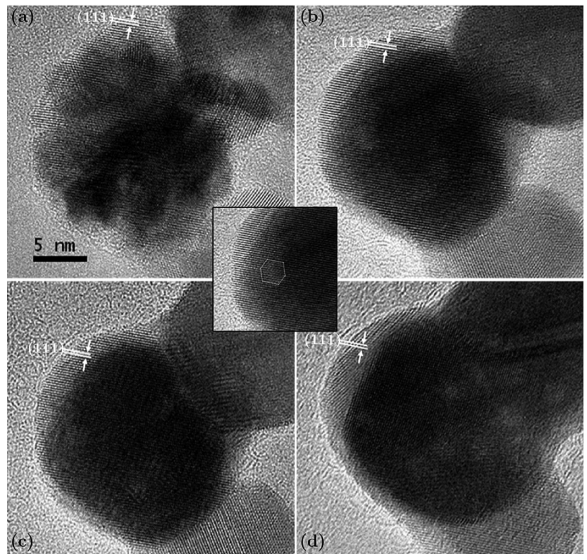

Figure 3. Selected temperature sequence of a nanoparticle, taken in situ in an aberration-corrected TEM at 300 kV: (a) room temperature, (b) 400, (c) 500, and (d) 600 °C. The inset shows the enlarged image of (b).

dx.doi.org/10.1021/jz3001823 | J. Phys. Chem. Lett. 2012, 3, 1106−1110

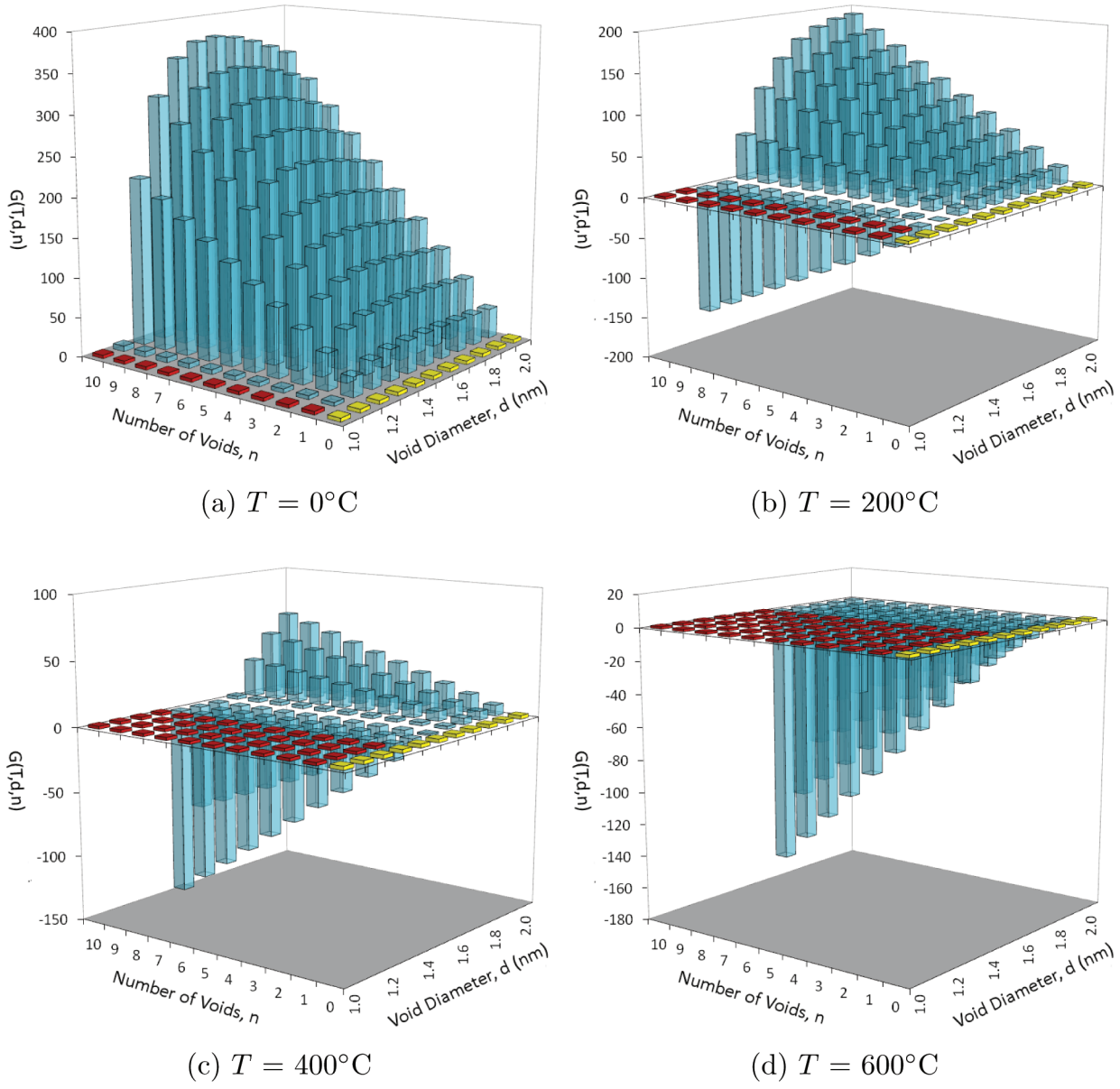

Figure 4. The total free energy, $G(T,d,n)$ in kJ/mol, of different void configurations at various temperatures (indicated). Yellow bars represent the solid nanoparticle having the same mass (no voids), and the red bars represent configurations where the interfaces have melted and the voids have collapsed.

For example, at 400 °C, once again, the irregular surface of the as-synthesized nanoparticle has become smooth and well-faceted, and voids approximately 1.5−2 nm in size have formed within the particle (Figure 3b). Upon increasing the temperature to 600 °C, the particle has sintered with nearby particles, and the voids have migrated to form larger voids (Figure 3d).

A more detailed analysis reveals that the voids formed at higher temperatures are faceted. As shown in the inset of Figure 3, an enlarged image of Figure 3b, the shapes of the voids are truncated octahedra with {111} and {100} surfaces. Similar trends regarding the shape, size, coalescence, and migration of voids described here have been observed in aged platinum foils annealed at temperatures between 250 and 500 °C.[30] Although the void formation mechanisms are different for platinum nanoparticles and aged foils, the agreement in the shapes and sizes of voids supports the formation of voids in platinum as a general phenomenon.

The existence and stabilities of voids in the nanoparticles have general implications for developing an understanding of the stability of porous nanoparticles, including the hollow- and mesoporous-structured ones. To this end, we have undertaken thermodynamic modeling based on parameters obtained from first-principles computer simulations. By using a theoretical approach, it is possible to predict the optimal void size and fraction under different conditions and to understand the sintering of the voids as the nanoparticles equilibrate. The shape-dependent thermodynamic model used here includes contributions from the particle bulk and surfaces[31] (see the Supporting Information for details). This model has previously proven successful in predicting the size- and temperature-dependent shapes of gold[32] and platinum[23,24] nanoparticles, without necessitating a large number of explicit simulations of individual structures.[33] The inclusion of voids within nanoparticles has been achieved by adding a contribution from the

dx.doi.org/10.1021/jz3001823 | J. Phys. Chem. Lett. 2012, 3, 1106−1110

void/particle interface to the total free energy of the system. The contribution from the voids is additive, and each void is characterized by its own (negative) surface-to-volume ratio but is still enclosed by {111} and {100} "facets", as observed experimentally. Void surfaces are referred to as *interfaces* to distinguish them from the external *surfaces* enclosing the nanoparticle. Just as the free energy (G) of the final nanoparticle is proportional to the surface-to-volume ratio, q, and the weighted sum of the free surface energies ($\sum_i f_i\gamma_i$) (where f_i is the fractional surface area of facet i and γ_i is the free energy of facet i), so too is the free energy associated with the voids (G') proportional to the interface-to-volume ratio, q', and the weighted sum of the interface energies ($\sum_i f_i'\gamma_i'$). In the simulations, the shape of the nanoparticle and the shapes of the individual voids have been optimized as a function of temperature, with the total mass of the system kept constant. This means that the diameter (D) of the nanoparticle increases proportionally when we introduce more voids or larger voids and may be easily calculated using

$$\langle D\rangle = 2\left[\frac{3(M/\rho) + 4/3n\pi(d/2)^3}{4\pi}\right]^{1/3} \quad (1)$$

where ρ is the density of platinum, M is the mass, the average diameter of the voids is denoted by d, and the number of voids per nanoparticle is denoted by n. For a total mass equivalent to the nineteen 5.5 nm octahedral primary nanoparticles, the stability of the different void configurations, calculated as the total free energy of the system, is shown in Figure 4. In these graphs, the yellow bars represent the completely solid nanoparticle (no voids), and the red bars represent configurations where the interfaces have melted and the voids have collapsed. In other words, the voids are beneath the size-dependent melting temperatures and cannot maintain the integrity necessary to exist at these configurations. At low temperature (Figure 4a), 1.0 nm voids have already collapsed, and all other void sizes are unstable with respect to a solid nanoparticle (irrespective of the void fraction).

However, as the temperature increases, we see an increased stability for certain void configurations. At T = 200 °C, in Figure 4b, a particle containing voids between 1.2 and 1.3 nm is more stable than a solid particle, particularly when the number of voids is high. This is due to a combination of factors. As mentioned above, as the number of voids increases, the overall diameter of the particle increases, and the external surface-to-volume ratio decreases to preserve the volume; therefore, the contribution from the sum of the external surfaces is reduced. There is an added contribution from the interfaces, but when they are very close to the size-dependent melting temperature, this contribution is insufficient to compensate the change in the external surface energy. When the voids are larger, this contribution overcompensates, and the configuration is thermodynamically unfavorable once more. Only those voids that have the appropriate size can compensate for the reduction of the contributions from external surface free energies.

At still higher temperatures, such as those shown in Figure 4c and d, larger voids become stable due to the same combination of contributions from the interfaces and the reduction in the external surface-to-volume ratio. Under these conditions, larger voids are close to the size-dependent melting temperature, and smaller voids have collapsed. This means that while there is always a small range of void sizes that is thermodynamically stable, the stable sizes increase with increasing temperature, and the voids sinter so that the entire nanoparticle can adopt the most stable configuration.

The stabilities of voids within nanoparticles at high temperatures (>200 °C), predicted by the theoretical calculations, support our experimental observations. The stable sizes of the voids, from approximately 1.2 to 2 nm for temperatures from 200 to 600 °C, are in good agreement with the experimental measurements. By combining both the experimental and the theoretical results, we have shown that porous platinum nanoparticles are relatively stable below ∼200 °C. At higher temperatures, the primary particles sinter, the irregular external morphology of porous nanoparticles changes to faceted surfaces, and the particles therefore lose their high external surface areas. However, the voids are present and stable in the interior of the particles. We anticipate that such behavior is general for porous metal particles of different configurations. That is, sintering happens at high temperatures so that the porous particles transform into faceted particles, but voids can be stable within the particles to maintain a thermodynamically favorable hollow structure. Such behavior can be used as an indication of the thermal stability of hollow-structured nanoparticles. When engineered with an appropriate void-to-total volume ratio, the hollow nanoparticles can be stable beyond 200 °C, so that it is possible to preserve their porosity at elevated temperatures. Considering the high cost of platinum, the presence and the stability of the voids in platinum particles at high temperatures could provide an economic advantage for the application of platinum-based catalysts.

■ ASSOCIATED CONTENT

Supporting Information

Detailed description of the characterization and modeling method. This material is available free of charge via the Internet at http://pubs.acs.org.

■ AUTHOR INFORMATION

Corresponding Author

*E-mail: shery.chang@monash.edu (S.L.Y.C.); amanda.barnard@csiro.au (A.S.B.).

Notes

The authors declare no competing financial interest.

■ ACKNOWLEDGMENTS

S.L.Y.C. acknowledges the support of the Early Career Research Grant funded by Monash University. The use of an aberration-corrected Titan^3 funded through ARC Grant No. LE0454166 is acknowledged. A.S.B acknowledges support from the Australian Research Council under Grant Number DP0986752 and computational resources supplied by the National Computing Infrastructure (NCI) national facility under MAS Grant p00. The A. P. Møller and Chastine McKinney Møller Foundation is gratefully acknowledged for their contribution towards the establishment of the Center for Electron Nanoscopy at the Technical University of Denmark. H.K. and H.F.X. acknowledge support from the NASA Astrobiology Institute (N07-5489), NSF (EAR-095800), and U.S. Department of Energy (DE-FG02-09ER16050).

■ REFERENCES

(1) Searles, R. Contribution of Automotive Catalytic Converters. In *Material Aspects in Automotive Catalytic Converters*; Bode, H., Ed.; Wiley: New York, 2002.

(2) Garry, J. H.; Handwerk, W. E. *Petroleum Refining Technology and Economics*, 4th ed.; Marcel Dekker: New York, 2001.
(3) Zhong, C. J.; Luo, J.; Fang, B.; Wanjala, B. N.; Njoki, P. N.; Loukrakpam, R.; Yin, J. Nanostructured Catalysts in Fuel Cells. *Nanotechnology* **2010**, *21*, 062001−062010.
(4) Watanabe, M.; Uchida, H. Electrocatalysis at Platinum and Bimetallic Alloys. In *Fuel Cell Catalysis: A Surface Science Approach*; Theodorus, M., Koper, M., Eds.; Wiley: New York, 2009.
(5) Vajda, S.; Pellin, M. J.; Greeley, J. P.; Marshall, C. L.; Curtiss, L. A.; Ballentine, G. A.; Elam, J. W.; Catillon-Mucherie, S.; Redfern, P. C.; Mehmood, F.; Zapo, P. Subnanometre Platinum Clusters as Highly Active and Selective Catalysts for the Oxidative Dehydrogenation of Propane. *Nat. Mater.* **2009**, *8*, 213−216.
(6) Yamamoto, K.; Imaoka, T.; Chun, W. J.; Enoki, O.; Katoh, H.; Takenaga, M.; Sonoi, A. Size-Specific Catalytic Activity of Platinum Clusters Enhances Oxygen Reduction Reactions. *Nat. Chem.* **2009**, *1*, 397−402.
(7) Grass, M. E.; Yue, Y.; Habas, S. E.; Rioux, R. M.; Teall, C. I.; Yang, P.; A., S. G. Silver Ion Mediated Shape Control of Platinum Nanoparticles: Removal of Silver by Selective Etching Leads to Increased Catalytic Activity. *J. Phys. Chem. C* **2008**, *112*, 4797−4804.
(8) Ren, J.; Tilley, R. D. Shape-Controlled Growth of Platinum Nanoparticles. *Small* **2007**, *3*, 1508−1512.
(9) Ahmadi, T. S.; Wang, Z. L.; Green, T. C.; Henglein, A.; El-Sayed, M. A. Shape-Controlled Synthesis of Colloidal Platinum Nanoparticles. *Science* **1996**, *272*, 1924−1925.
(10) Guczi, L. Bimetallic Nano-Particles: Featuring Structure and Reactivity. *Catal. Today* **2005**, *101*, 53−64.
(11) Ferrando, R.; Jellinek, J.; Johnston, R. L. Nanoalloys: From Theory to Applications of Alloy Clusters and Nanoparticles. *Chem. Rev.* **2008**, *108*, 845−910.
(12) Ponec, V. Surface Chemistry and Catalysis on Some Platinum-Bimetallic Catalysts. In *Catalyst Characterization Science: surface and solid state chemistry*; Deviney, M. L., Gland, J. L., Eds.; American Chemical Society: Washington DC, 1985.
(13) Attard, G. S.; Bartlett, P. N.; Coleman, N. R. B.; Elliott, J. M.; Owen, J. R.; Wang, J. H. Mesoporous Platinum Films from Lyotropic Liquid Crystalline Phases. *Science* **1997**, *278*, 838−840.
(14) Wang, L.; Yamauchi, Y. Block Copolymer Mediated Synthesis of Dendritic Platinum Nanoparticles. *J. Am. Chem. Soc.* **2009**, *131*, 9152−9153.
(15) Song, Y.; Yang, Y.; Medforth, C. J.; Pereira, E.; Singh, A. K.; Xu, H.; Jiang, Y.; Brinker, C. J.; van Swol, F.; Shelnutt, J. A. Controlled Synthesis of 2-D and 3-D Dendritic Platinum Nanostructures. *J. Am. Chem. Soc.* **2003**, *126*, 635−645.
(16) Chen, H. M.; Liu, R. S.; Lo, M. Y.; Chang, S. C.; Tsai, L. D.; Peng, Y. M.; Lee, J. F. Hollow Platinum Spheres with Nano-Channels: Synthesis and Enhanced Catalysis for Oxygen Reduction. *J. Phys. Chem. C* **2008**, *112*, 7522−7526.
(17) Liang, H.; Zhang, H.; Hu, J.; Guo, Y.; Wan, L.; Bai, C. Pt Hollow Nanospheres: Facile Synthesis and Enhanced Electrocatalysts. *Angew. Chem., Int. Ed.* **2004**, *43*, 1540−1543.
(18) Sun, B. Y.and Brian Mayers; Xia, Y. Metal Nanostructures with Hollow Interiors. *Adv. Mater.* **2003**, *15*, 641−646.
(19) Teng, X.; Liang, X.; Maksimuk, S.; Yang, H. Synthesis of Porous Platinum Nanoparticles. *Small* **2006**, *2*, 249−253.
(20) Yang, D.; Sun, S.; Meng, H.; Dodelet, J.; Sache, E. Formation of a Porous Platinum Nanoparticle Froth for Electrochemical Applications, Produced without Templates, Surfactants, or Stabilizers. *Chem. Mater.* **2008**, *20*, 4677−4681.
(21) Pasricha, R.; Bala, T.; Biradar, A. V.; Umbarkar, S.; Sastry, M. Synthesis of Catalytically Active Porous Platinum Nanoparticles by Transmetallation Reaction and Proposition of the Mechanism. *Small* **2009**, *12*, 1467−1473.
(22) Meyer, D. A.; Oliver, J. A.; Albrecht, R. M. Detection of Nanoparticles of Differing Composition for High Resolution Labeling. *Microsc. Microanal.* **2010**, *16*, 992−993.
(23) Barnard, A. S.; Chang, L. Y. Thermodynamic Cartography and Structure/Property Mapping of Commercial Platinum Catalysts. *ACS Catal.* **2011**, *1*, 76−81.
(24) Chang, L. Y.; Cervera Gontard, L.; Dunin-Borkowski, R. E.; Ozkaya, D. Resolving the Structure of Active Sites on Platinum Catalytic Nanoparticles. *Nano Lett.* **2010**, *10*, 3073−3076.
(25) Cervera Gontard, L.; Chang, L. Y.; Hetherington, C. J. D.; Kirkland, A. I.; Ozkaya, D.; Dunin-Borkowski, R. E. Aberration-Corrected Imaging of Active Sites on Industrial Catalyst Nanoparticles. *Angew. Chem., Int. Ed.* **2007**, *46*, 3683−3685.
(26) Cervera Gontard, L.; Dunin-Borkowski, R. E.; Ozkaya, D. Three-Dimensional Shapes and Spatial Distributions of Pt and PtCr Catalyst Nanoparticles on Carbon Black. *J. Microsc.* **2008**, *232*, 248−259.
(27) Peng, Z.; Yang, H. Designer Platinum Nanoparticles: Shape, Composition in Alloys, Nanostructure and Electrocatalytic Property. *Nano Today* **2009**, *4*, 143−164.
(28) Sau, T. K.; Rogach, A. L. Nonspherical Noble Metal Nanoparticles: Colloid-Chemical Synthesis and Morphology Control. *Adv. Mater.* **2010**, *22*, 1781−1804.
(29) Barnard, A. S.; Konishi, H.; Xu, H. F. Morphology Mapping of Platinum Catalysts over the Entire Nanoscale. *Catal. Sci. Technol.* **2011**, *1*, 1440−1448.
(30) Newman, R. W.; Hern, J. J. Secondary Defectsin Quenched and Aged Platinum. *Metall. Trans.* **1970**, *2*, 1129−1138.
(31) Barnard, A. S. Modelling of Nanoparticles: Approaches to Morphology and Evolution. *Rep. Prog. Phys.* **2010**, *73*, 086502−086522.
(32) Barnard, A. S.; Young, N. P.; Kirkland, A. I.; van Huis, M. A.; Xu, H. F. Nanogole: a Quantitative Phase Map. *ACS Nano* **2009**, *3*, 1431−1436.
(33) Barnard, A. S.; Curtiss, L. A. Predicting the Shape and Structure of Face-Centered Cubic Gold Nanocrystals Smaller than 3 nm. *ChemPhysChem* **2006**, *7*, 1544−1553.